# Vortices in tunable dipolar Bose-Einstein condensates with attractive interactions

S. Sabari,[1] R. Sasireka,[2] R. Radha,[3] A. Uthayakumar,[2] and Lauro Tomio[1,4]
[1]*Instituto de Física Teórica, Universidade Estadual Paulista, 01140-070 São Paulo, São Paulo, Brazil*
[2]*Department of Physics, Presidency College (Autonomous), Chennai 600005, India*
[3]*Centre for Nonlinear Science, Department of Physics, Government College for Women (Autonomous), Kumbakonam 612001, India*
[4]*Centro Internacional de Física, Instituto de Física, Universidade de Brasília, 70910-900 Brasília, Distrito Federal, Brazil*

(Received 16 January 2025; accepted 12 May 2025; published 30 May 2025)

We investigate the formation of vortices in quasi-two-dimensional dipolar Bose-Einstein condensates (BECs) through the interplay between two-body contact and long-ranged dipole-dipole interactions (DDIs), as both interactions can be tuned from repulsive to attractive. By solving the associated Gross-Pitaevskii equation for a rotating system, our initial approach concentrates on stabilizing a collapsing condensate with attractive *s*-wave two-body interactions by employing sufficiently large repulsive DDIs. Subsequently, the same procedure was applied after reversing the signs of both interactions to evaluate the sensitivity of vortex formation to such an interchange of interactions. As a reference to guide our investigation, valid for generic dipolar atomic species, we have assumed a condensate with the strong dipolar dysprosium isotope, $^{164}$Dy. The correlation of the results with other dipolar BEC systems was exemplified by considering rotating BECs with two other isotopes, namely $^{168}$Er and $^{52}$Cr. For a purely dipolar condensate (no contact interactions) under fixed rotation, we show how the number of visible vortices increases as the DDI becomes more repulsive, accomplished by tuning the orientation of the dipoles through a characteristic angle parameter.

DOI: 10.1103/PhysRevA.111.053320

## I. INTRODUCTION

Superfluidity, which is believed to be a remarkable macroscopic quantum phenomenon, was discovered in the investigation of liquid helium by Kapitza [1] and Allen and Misener [2]. They showed that liquid He can flow without viscosity below a critical temperature. Liquid helium remained the only bosonic liquid realized in an experiment until 1995. The advent of laser cooling with dilute alkali-metal atoms resulted in the experimental realization of the new phase of matter called the "Bose-Einstein condensate" (BEC) [3]. The BEC turns out to be a new addition to the family of superfluid, which is strikingly different from liquid He, the first member of this family. Liquid helium is a strongly interacting system which makes its theoretical description extremely difficult. It has no system parameters like density and interaction strength which can be manipulated experimentally. In addition, it has no spin degrees of freedom. On the other hand, almost all the parameters like density, kinetic energy, and interaction strengths in BECs can be manipulated experimentally by engineering the atom laser interaction strength in magnetic or optical traps using Feshbach resonance techniques [4]. By choosing atomic species and employing optical traps to release the spin degrees of freedom, one can realize the spinor superfluid [5–7] and the dipolar superfluid [8]. Another advantage of BECs is that ultracold gases are dilute and weakly interacting systems which means that they can be easily described by mean-field approximation governed by the usual Gross-Pitaevskii (GP) equation or its generalizations.

It should be pointed out that the nonlinearity in a BEC arises by virtue of the two-body short-range *s*-wave contact interaction. However, realizations of BECs with long-range dipolar atoms have opened up plenty of avenues leading to new possibilities in the domain of ultracold atoms. Dipolar atoms are characterized by having long-range anisotropic interactions with the first BEC realizations reported with isotopes of chromium [8] followed by dysprosium [9] and erbium [10]. Far from being different from the isotropic contact interaction in condensates with alkali-metal atoms, it is expected that dipole-dipole interaction (DDI) can lead to new ground-state properties and interesting phenomena. Recent experiments have shown that dipolar BECs can form supersolid states of matter [11–13]. Further, dipolar BECs have been endowed with the possibility of playing with two different kinds of interactions in a dilute system, namely, the conventional two-body contact and the long-range dipolar interactions, with possibilities to be tuned from attractive to repulsive. Such dynamical systems associated with BECs have been theoretically and experimentally explored in different perspectives, as exemplified by Refs. [14–32]. Concerned with dipolar binary mixtures, several investigations have been done, such as by exploring miscibility properties with different dipolar species [33–37]. Also, one can trace the actual interest on dipolar mixtures from the recent experimental reports on condensation of dipolar molecules [38], and on the production of spin mixtures with Zeeman sublevels of $^{162}$Dy [39].

Relevant to the phenomenon of superfluidity, "quantized vortices" have also been intensively investigated before in nondipolar quantum gas experiments, as also for binary coupled BECs in Refs. [40,41] (and references therein), with their occurrence in dipolar atoms being reported only recently in Ref. [42]. Vortices are considered to be the hallmark of

 

superfluidity representing the breakdown of laminar flow with their identification having wider ramifications for understanding quantum turbulence [43]. With the experimental realization of BECs using dipolar atomic isotopes, there has been significant laboratory investigation into vortices in dipolar BECs and their corresponding properties, as recently discussed in Ref. [44]. In a BEC, a vortex is described by a solution of the GP equation that carries angular momentum governed by the geometry and dimensionality of the system under consideration. A one-dimensional BEC strictly cannot sustain a vortex solution and can support only solitons [45]. While classical vortices can take any value of circulation, superfluids are irrotational such that angular rotation is constrained to occur through vortices with quantized circulation known as "quantized vortices."

In the BECs realized with alkali-metal atoms, the density of the atoms is of the order of $10^4$ atoms/cc. At such densities, the interaction between the atoms is weak and predominantly described by $s$-wave scattering lengths $a_s$, which being positive indicates repulsive interaction. In such cases, with $a_s > 0$, there is no upper limit to the number of atoms occupying a stable configuration, which can have more than $1 \times 10^6$ atoms. This is the situation with $^{87}$Rb [3] and $^{23}$Na [46]. However, if the scattering length becomes negative, the interaction between the atoms is attractive, implying that there is an upper limit to the number of atoms of a stable condensate as verified experimentally in the case of $^{7}$Li [47]. In addition, it is well understood that vortices are more energetically favored with repulsive interactions. This underscores the fact that the identification of vortices in rotating BECs with attractive two-body interactions continues to be challenging [48–51], with their existence relying on shape deformations of the trap. Atomic intrinsic properties other than two-body contact interaction can also provide the necessary stability of a condensate against collapse, as shown in Refs. [52–55].

Hence, the main focus of the present paper is to explore the possibility of generating vortices in dipolar BEC systems having attractive contact interactions with large enough repulsive DDI. Consistently with the stability analysis performed in Refs. [56,57] within the Thomas-Fermi limit approximation, in our full numerical approach, we are assuming a quasi-two-dimensional (2D) large trap anisotropy. The specific role of each kind of interaction in vortex production is further investigated by inverting the sign of short- and long-range interactions with the stability being accomplished in attractive dipolar systems by the reinforcement of repulsive contact interaction.

This paper is organized as follows. In Sec. II, we present the quasi-2D mean-field description to portray the dynamics of dipolar BECs with two-body contact interactions. It is pointed out how one can manipulate experimentally the sign of both interactions independently. In Sec. III, we present our main results, assuming a hypothetical dipolar BEC, in two subsections (Secs. III A and III B), by considering the DDI strongly repulsive (Sec. III A) and attractive (Sec. III B), with the associated contact interactions having opposite signs, being attractive (or close to zero) in Sec. III A and sufficiently repulsive in Sec. III B. In Sec. IV, by assuming three atomic samples for the BECs, we establish a correlation between the $^{164}$Dy, $^{168}$Er, and $^{52}$Cr condensates. Finally, our main conclusions are highlighted in Sec. V.

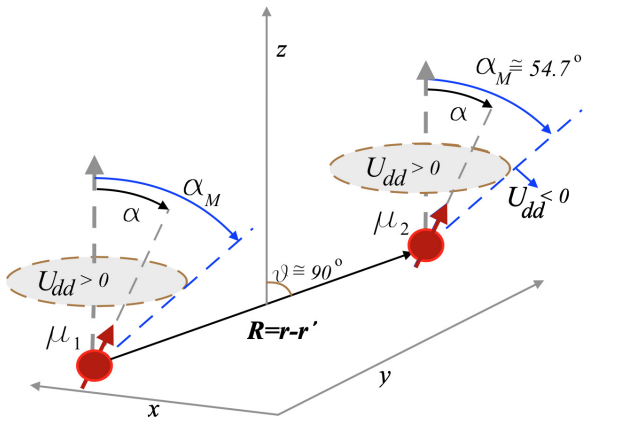


FIG. 1. Illustration of the dipole-dipole interaction, as given by (2), where $\boldsymbol{\mu}_1 = \boldsymbol{\mu}_2 = \boldsymbol{\mu}$, with $\alpha$ being the dipole orientations related to the $z$ axis which we assume to tune the strength and sign of the effective dipole-dipole interaction.

## II. THE MODEL

A trapped ultracold short-ranged $s$-wave weakly interacting dipolar gas of bosonic atoms in a rotating system can be described by the following three-dimensional (3D) time-dependent extension of the GP mean-field formalism [14,17,20] for the corresponding wave function $\phi(\mathbf{r}, t)$:

$$i\hbar\frac{\partial\phi(\mathbf{r},t)}{\partial t} = \Big[-\frac{\hbar^2}{2m}\nabla^2 + V(\mathbf{r}) - \Omega L_z + g_s|\phi(\mathbf{r},t)|^2 + N\int U_{dd}(\mathbf{r}-\mathbf{r}')|\phi(\mathbf{r}',t)|^2 d\mathbf{r}'\Big]\phi(\mathbf{r},t), \quad (1)$$

where $\phi(\mathbf{r}, t)$ is normalized to 1, $\hbar$ is the reduced Planck's constant, $m$ is the atom mass, and $N$ is the number of total condensed atoms. $V(\mathbf{r})$ is the trap potential which we assume given by a nonsymmetric 3D harmonic interaction $V(\mathbf{r}) = \frac{1}{2}m\omega_\rho^2[(x^2 + y^2) + \lambda z^2]$, where $\omega_x = \omega_y = \omega_\rho$ with $\lambda \equiv (\omega_z/\omega_\rho)^2$ being the shape parameter. With the condensate rotating about the $z$ axis with angular velocity $\Omega$, $L_z \equiv -i\hbar(x\frac{\partial}{\partial y} - y\frac{\partial}{\partial x})$ will correspond to the $z$ component of the total angular momentum operator. The nonlinear contact and dipolar interactions are respectively given by the last two terms within the square brackets of Eq. (1). The strength of the two-body interaction given in terms of the two-body scattering length $a_s$, $g_s \equiv 4\pi\hbar^2 a_s N/m$, can be tuned from attractive (negative) to repulsive (positive) values by employing Feshbach resonance techniques [4]. The long-range interaction between two polarized magnetic dipoles located at $\mathbf{r}$ and $\mathbf{r}'$ as illustrated in Fig. 1, can be expressed by [56]

$$U_{dd}(\mathbf{r}-\mathbf{r}') = \frac{\mu_0\mu^2(1-3\cos^2\vartheta)}{4\pi}\frac{(3\cos^2\alpha - 1)}{2|\mathbf{r}-\mathbf{r}'|^3}, \quad (2)$$

where $\mu_0$ is the permeability of free space, $\vartheta$ is the angle between the $z$ axis and the vector position of the dipoles $\mathbf{R} \equiv \mathbf{r} - \mathbf{r}'$, and $\alpha$ defines the angle of inclination of both dipole moments $\boldsymbol{\mu}$ relative to the $z$ direction. In our approach,

we consider pancakelike confinement with $\lambda \gg 1$ such that most of the atoms are close to the transverse plane. Therefore, the vector position of dipoles $\mathbf{R}$ can be assumed to be close to a plane perpendicular to the $z$ direction or $\vartheta \approx 90^\circ$ (with the exact limit being considered in the present 2D case). For more details, see Refs. [58,59] where this formalism was considered for vortex production and to study the turbulent dynamics in dipolar systems. Therefore, the angle $\alpha$ describing the orientation of the dipoles related to the $z$ axis turns out to be the key parameter in Eq. (2) to manipulate and effectively alter the DDI. With $\alpha_M \approx 54.7^\circ$ being the *magic angle* at which the DDI vanishes (independently of $\mu$), the DDI can vary from repulsive (when $\alpha < \alpha_M$) to attractive (when $\alpha > \alpha_M$) interactions.

For the convenience of using the GP equation (1) in dimensionless form, we introduce the dimensionless variables with the length and time units given by $\ell_\rho = \sqrt{\hbar/(m\omega_\rho)}$ and $\omega_\rho^{-1}$. With this procedure, the previous physical quantities are transformed as $\bar{\mathbf{r}} = \mathbf{r}/\ell_\rho$, $\bar{\mathbf{R}} = \mathbf{R}/\ell_\rho$, $\bar{t} = t\omega_\rho$, $\bar{\phi} = \ell_\rho^{3/2}\phi$, $\bar{\Omega} = \omega_\rho^{-1}\Omega$, and $\bar{V} = \hbar\omega_\rho V$ with Eq. (1) expressed in terms of the overhead bar variables. By removing the overhead bar from all the variables (which will be understood as dimensionless), Eq. (1) can be written as

$$i\frac{\partial\phi(\mathbf{r},t)}{\partial t} = \Bigg[-\frac{\nabla^2}{2} + V(\mathbf{r}) - \Omega L_z + g_{3D}|\phi(\mathbf{r},t)|^2 + g_{dd}\int \frac{3\cos^2\alpha - 1}{2|\mathbf{r}-\mathbf{r}'|^3}|\phi(\mathbf{r}',t)|^2 d\mathbf{r}'\Bigg]\phi(\mathbf{r},t), \tag{3}$$

where $g_{3D} \equiv 4\pi N a_s/\ell_\rho = g_s/(\hbar\omega_\rho\ell_\rho^3)$ and $g_{dd} \equiv N\mu_0\mu^2/(4\pi\hbar\omega_\rho\ell_\rho^3)$. In terms of a defined dipole length $a_{dd} \equiv \mu_0\mu^2 m/(12\pi\hbar^2)$, we can write $g_{dd} = 3N(a_{dd}/\ell_\rho)$. The stability of a dipolar BEC depends on the external trap geometry. For example, a dipolar BEC is stable or unstable depending on whether the trap is pancake or cigar shaped, respectively. The instability usually can be overcome by applying a strong pancake trap with repulsive two-body contact interaction. The external trap helps to stabilize the dipolar BEC by imprinting anisotropy onto the density distribution. Hence, with the dynamics of the dipolar BEC being strongly confined in the axial direction ($\lambda \gg 1$), $\Psi(\mathbf{r},t)$ can be decoupled as

$$\phi(\mathbf{r},t) \equiv \chi(z)\psi(\boldsymbol{\rho},t) \equiv \left(\frac{\lambda}{\pi}\right)^{1/4}\exp\left(\frac{-\lambda z^2}{2}\right)\psi(\boldsymbol{\rho},t), \tag{4}$$

where $\boldsymbol{\rho} \equiv (x,y) \equiv (\rho\cos\vartheta, \rho\sin\vartheta)$ allowing $z$ to be integrated out. After simplification, we obtain the effective 2D pancake-shaped dipolar BEC [33,60] as

$$\mathrm{i}\frac{\partial\psi(\boldsymbol{\rho},t)}{\partial t} = \Bigg\{-\frac{1}{2}\nabla_\rho^2 + \frac{\rho^2}{2} - \Omega L_z + g_{2D}|\psi(\boldsymbol{\rho},t)|^2 + g_{dd}\int \frac{d^2k_\rho}{4\pi^2}e^{i\mathbf{k}_\rho\cdot\boldsymbol{\rho}}\widetilde{n}(\mathbf{k}_\rho)\widetilde{V}^{(d)}(\mathbf{k}_\rho)\Bigg\}\psi(\boldsymbol{\rho},t), \tag{5}$$

where $g_{2D} \equiv \sqrt{8\pi\lambda}(a_s/\ell_\rho)N$. In the above 2D Eq. (5), $\widetilde{n}(\mathbf{k}_\rho)$ and $\widetilde{V}^{(d)}(\mathbf{k}_\rho)$ are the Fourier transforms of the 2D density and dipolar potential respectively. As shown in Refs. [58,59], the DDI in momentum space after an averaging of the polarization rotating field in the $(k_x, k_y)$ plane can be expressed as

$$\widetilde{V}^{(d)}(\mathbf{k}_\rho) = \frac{3\cos^2\alpha - 1}{2}\left[2 - 3\sqrt{\frac{\pi}{2\lambda}}k_\rho e^{\frac{k_\rho^2}{2\lambda}}\mathrm{erfc}\left(\frac{k_\rho}{\sqrt{2\lambda}}\right)\right] \tag{6}$$

where $\mathrm{erfc}(x)$ is the complementary error function of $x$. Therefore, as shown above, the strength of the atom-atom long-ranged dipolar interaction is guided by the factor $g_{dd}(3\cos^2\alpha - 1)/2$ which varies from $g_{dd}$ for $\alpha = 0^\circ$ to $-g_{dd}/2$ for $\alpha = 90^\circ$ while it vanishes for $\alpha \approx 54.7^\circ$. In other words, by changing the orientation of the dipoles with the $z$ axis, one can change not only the magnitude of DDI but also the direction changing the interaction from repulsive to attractive as well. So, restricted by possible stability requirements, the two kinds of nonlinear interactions present in Eq. (5) (short- and long-ranged ones), in principle, can be manipulated independently: In other words, for the contact interaction, we have the Feshbach techniques to change $a_s$ from attractive to repulsive, and for the DDI (as shown in Fig. 1), we have the orientations of the two dipoles defined by the angle $\alpha$ (once considered $\vartheta$ fixed at $90^\circ$). In terms of $\alpha$, we can assume the DDI strength to be redefined as

$$a_{dd}(\alpha) = a_{dd}\frac{3\cos^2\alpha - 1}{2}, \tag{7}$$

so that it can vary from maximum repulsive [$a_{dd}\ (0^\circ) = a_{dd}$] to maximum attractive [$a_{dd}(90^\circ) = -a_{dd}/2$].

For the numerical solution of Eq. (5) to investigate the vortex formation in the condensate, we have combined the usual split-step Crank-Nicholson method together with the fast Fourier-transform approach. In our numerics, we have used a $512 \times 512$ grid size with $\Delta x = \Delta y = 0.04$ for both $x$ and $y$ (units $\ell_\rho$) with time step $\Delta t = 0.01$ (units $\omega_\rho^{-1}$). Assuming initially the strong dipolar dysprosium isotope $^{164}$Dy as the hypothetical atomic sample in our investigation, we kept the number of atoms fixed at $N = 1.0 \times 10^3$ with the rotational frequency being $\Omega = 0.9$ (units $\omega_\rho$) and the length unit such that $\ell_\rho = 1 \times 10^{-6}m$. In this case, $a_{dd} \approx 6.94 \times 10^{-3}\ell_\rho \approx 131\,a_0$, where $a_0 = 0.529\,18 \times 10^{-10}m$ is the Bohr radius. In order to compare with other dipolar BECs made up of erbium and chromium isotopes, the long-range DDI can be kept at $a_{dd} \approx 66\,a_0$ ($^{168}$Er) and $a_{dd} \approx 16\,a_0$ ($^{52}$Cr) respectively. For all vortex studies, we first prepare a stable initial state using imaginary time propagation. Subsequently, by introducing the rotational frequency $\Omega$, we evolve the system in real time by using the split-step Crank-Nicholson method.

By exploiting the characteristics of a rotating dipolar BEC confined in a quasi-2D harmonic trap, the rotational frequency has been set to a high value, $\Omega = 0.9$ (in units of $\omega_\perp$). This value is close to the critical limit yet remains below the maximum frequency allowed by the trap, enabling the formation of vortices. In dipolar BECs, the critical rotation frequency required to nucleate vortices is generally lower than the trapping frequency [61,62]. Several studies have explored the behavior of these critical frequencies in the presence of both DDI and conventional contact interactions, with Refs. [17,23,29,30] offering comprehensive analyses.

The critical values are strongly influenced by the trap geometry and the relative strengths of the interactions. In the present paper, stable vortex patterns have been generated and investigated by choosing contact and dipolar interactions with opposite signs and by setting the rotation frequency to $\Omega = 0.9$.

## III. VORTEX FORMATION IN DIPOLAR BECS WITH ATTRACTIVE INTERACTIONS

In this section, we study the interplay between long- and short-range interactions with one of these interactions being attractive. For that, we have numerically analyzed the corresponding energetic parameters and rotational properties of the condensates. In Sec. III A, our primary objective was to stabilize a collapsing condensate with attractive $s$-wave interactions using a sufficiently large repulsive DDI. This was followed by an analysis of vortex generation at a rotational frequency $\Omega = 0.9$, which is close to the transverse trap frequency. In Sec. III B, we reversed the roles of the long- and short-range interactions, considering an attractive DDI. Starting with a nonrotating, stable BEC system, we subjected it to high rotation ($\Omega = 0.9$) and analyzed the sensitivity of vortex formation on the nature of the interactions.

### A. Attractive $s$-wave two-body interaction

The possibility of generating visible vortices in attractive BECs has been studied before for nondipolar systems with deformed trap configurations. In general, the term "visible vortices" refers to vortices that can be resolved through experimental imaging techniques. These vortices exhibit a well-defined phase structure that can be detected using interference methods commonly employed in BEC experiments. Consequently, vortex fluctuations occurring within regions of very low atomic density—detectable only through detailed phase analysis—are neglected in this paper, as they contribute negligibly to the system's angular momentum.

Even without rotation, the condensate stability is limited up to some critical number of atoms. By considering dipolar systems, our aim is to explore the vortex production while having attractive contact interaction which will be compensated with enough repulsive dipolar interactions. To highlight the impact of attractive short-range $s$-wave interaction on the vortex production, we first switch off completely the long-range DDI and consider the reduction of the $s$-wave two-body repulsive interaction. The results shown for the densities $|\psi|^2$ are presented in the upper panels of Fig. 2. Represented in Figs. 2(a)–2(c), we have $a_s$ being reduced from $a_s = 220\,a_0$ [Fig. 2(a)] to $a_s = -1\,a_0$ [Fig. 2(c)]. As shown in the previous section, this is realized in our approach by fixing the dipolar angle $\alpha$ at $\approx 54.7^\circ$ such that the dipolar condensate will behave like a nondipolar system. As a reference atomic sample, we consider a $^{164}$Dy BEC for our investigation. In Fig. 2(c), both interactions are close to zero with the nonlinearity still being maintained by a small negative $a_s$ which means that the binary interaction becomes attractive. In such a case, the condensate can exist only for a critical number of atoms [21,23,52] before it collapses. Here, we use a fixed rotational frequency with $\Omega = 0.9$, large enough to generate visible vortices in

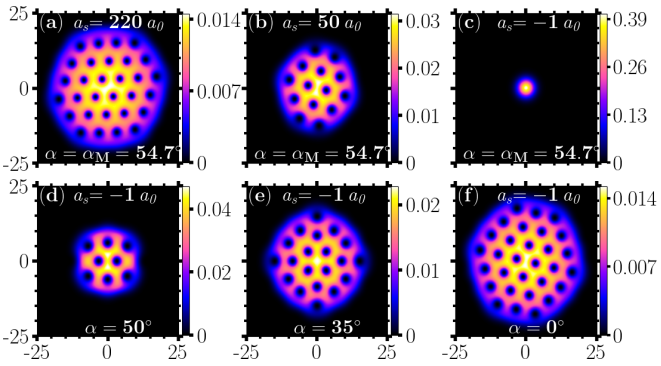


FIG. 2. Vortex patterns in $(x, y)$ density distributions given by $\Omega = 0.9$ (unit $\omega_\rho$) for a dipolar BEC in which $\alpha$ is the dipolar parameter controlling the strength as given by Eq. (7). In the upper panels, the DDI is set to zero by $\alpha = \alpha_M = 54.7^\circ$ with the contact interactions varying from repulsive, $a_s = 220\,a_0$ (a) and $a_s = 50\,a_0$ (b), to attractive $a_s = -1\,a_0$ (c). In the bottom panels, the contact interactions are kept attractive as in (c) with DDI being increasingly repulsive with $\alpha$ varying as $\alpha = 50^\circ$ (d), $\alpha = 35^\circ$ (e), and $\alpha = 0^\circ$ (f). The density levels are shown in bars at the right of each panel with the length unit being $\ell_\rho$.

condensates having enough distribution of the density within the trap. Actually, in a BEC with a rotating trap potential, visible vortices begin to appear only at a certain rotational frequency called critical frequency ($\Omega_c$) [29,30]. This implies that in BECs confined to a rotating trapping potential $\Omega < \Omega_c$, ghost vortices are first generated in the low-density region of the condensates and they do not carry any significant angular momentum. Also, at $\Omega = \Omega_c$, the ghost vortices start to enter the density region of the BECs and get transformed into visible vortices. From the results in Fig. 2(a), we see how visible vortices appear in the absence of DDI for repulsive binary interaction at $a_s = 220\,a_0$. By diminishing the strength of the short-ranged repulsive interaction, the number of visible vortices continuously decreases [Fig. 2(b)], while the density increases. This process continues till the area becomes too small to contain (or generate) a single vortex. At this juncture, by changing the binary contact interaction from repulsive to attractive, we end up with a situation where the density becomes so high and the area shrinks such that no vortices are allowed even with higher rotational frequencies. This is the general expected behavior for a nondipolar system in which the nonlinear contact interactions play the main role. However, considering a dipolar system in which the dipolar strength can be controlled through the angle $\alpha$, as given by (7), an obvious strategy is to generate vortices in the condensate by increasing the repulsive long-range interaction using $\alpha$ as a tuning parameter. This is exemplified in Figs. 2(d)–2(f) with $\alpha$ given by $50^\circ$, $35^\circ$, and $0^\circ$, respectively. The sensitivity of the dipolar interactions as related to the contact interactions can already be verified by comparing the upper panels (when DDI is set to zero) with the lower ones (when the contact interaction is attractive close to zero). Notice that just by changing about $4.7^\circ$ of the parameter $\alpha$, the dipolar condensate goes from zero vortices to display about eight vortices, as verified by going from Fig. 2(c) to Fig. 2(d). In this regard, another point to be noticed is the increase in the number of vortices for

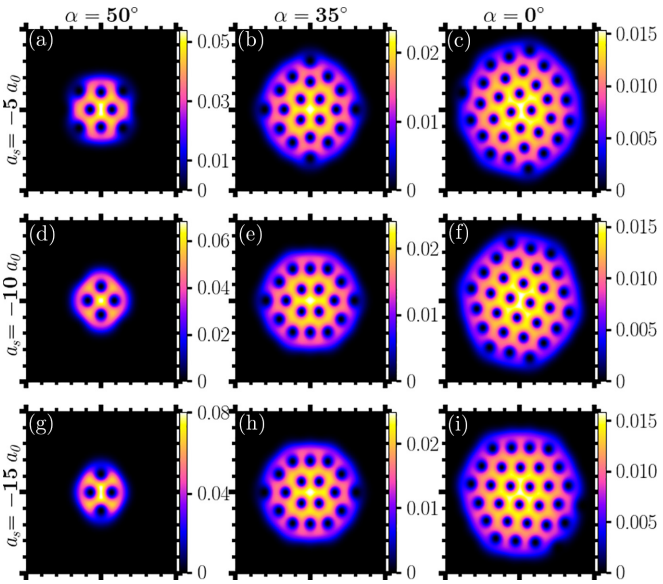


FIG. 3. With the same rotation, panel sizes, and units as in Fig. 2, here the vortex patterns are for a dipolar BEC with attractive contact interactions indicated at the left of the row sets ($a_s = -5\,a_0, -10\,a_0, -15\,a_0$). The DDI strengths (identified by $\alpha$) are fixed for each column with the maximum repulsive being $a_{dd}$ (0°) (= 131 $a_0$ for $^{164}$Dy).

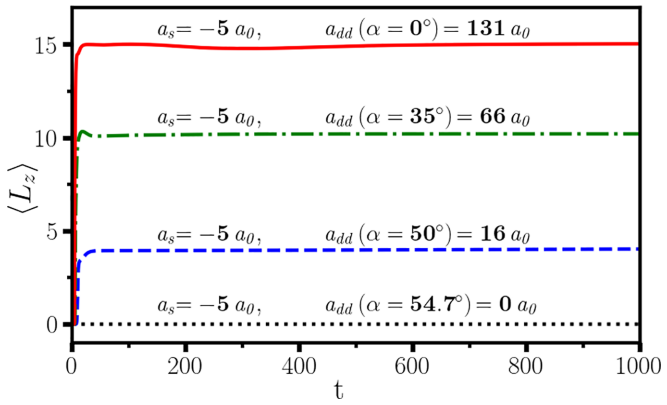


FIG. 4. Time evolution in units $\omega_\rho^{-1}$ of the averaged angular momentum per particle (units $\hbar$), along the vortex formation for $\Omega = 0.9$ (units $\omega_\rho$) and attractive contact interaction $a_s = -5\,a_0$ considering four different cases. To have maximum DDI, we assume the BEC to be made up of $^{164}$Dy.

pure repulsive contact interactions, which goes almost linearly from 0 to about 30 with $a_s$ varying from 0 $a_0$ [Fig. 2(c)] to 220 $a_0$ [Fig. 2(a)], whereas in the pure dipolar case, this happens for $\alpha$ decreasing from 54.7° [Fig. 2(c)] to 0° [Fig. 2(f)].

Hence, to demonstrate the vortex formation in the condensate with attractive two-body interaction, we start with the case in which the contact interaction is slightly negative with $a_s = -1\,a_0$, but with the DDI being repulsive, which is shown in Fig. 2(d) with $\alpha = 50°$. Next, as expected, more visible vortices are observed as we increase the repulsive DDI by decreasing the value of $\alpha$ with Figs. 2(e) and 2(f) showing the density distributions for $\alpha = 35°$ and 0°, respectively. Further, it is worth mentioning that the results for the $^{164}$Dy BEC with $\alpha = 50°$ and 35° are almost equal to the $^{52}$Cr and $^{168}$Er BECs respectively in their maximum DDI configurations once the masses and transversal trap frequencies are appropriately rescaled to fix the length unit (more details are provided at the end of this section and in Sec. IV).

Next, to verify the relative sensitivity in the results of the vortex pattern with changes provided by attractive contact interactions related to variations of the repulsive DDIs in Fig. 3, we have a set of panels with density results obtained with fixed $\Omega = 0.9$. At each row, the attractive contact interaction is fixed such that $a_s = -5\,a_0$ (top row), $a_s = -10\,a_0$ (middle row), and $a_s = -15\,a_0$ (bottom row) with the DDIs varying for each column of panels with $\alpha = 50°$ (left), $\alpha = 35°$ (middle), and $\alpha = 0°$ (right). It can be observed that once we fix the DDI, change of the contact interactions from $-5\,a_0$ to $-15\,a_0$ does not have any impact on the number of vortices and is more pronounced only for the case when the repulsive DDI is not large (as in case that $\alpha = 50°$). When the DDI is large enough, as in the second and third columns, we have almost no changes in the number of visible vortices for a variation of about 10 $a_0$ in the repulsive contact interactions.

Further, in Fig. 4, the stability of the generated vortices is examined by fixing the attractive short-range interaction at $a_s = -5\,a_0$ and varying the strengths of the DDI. This is achieved by considering different dipole orientation angles: $\alpha = 0°$ (maximum DDI), 35°, 50°, and 54.7° (zero DDI). The average angular momentum which gives a measure of stability is found to be maximum for a $^{164}$Dy BEC such that $a_{dd} = 131\,a_0$. The other two values for $\alpha = 35°$ and 50° refer to the maximum DDI of $^{168}$Er and $^{52}$Cr with $a_{dd} = 66\,a_0$ and $16\,a_0$ respectively. The stability of the produced vortices is probed by considering the time evolution of the averaged angular momentum per particle, $\langle L_z \rangle$, with the saturation of $\langle L_z \rangle$ representing the stability [22]. From Fig. 4, one observes that $\langle L_z \rangle$ for $\alpha = 0°$ is found to be maximum compared to that of $\alpha = 35°$ and 50°. When $\alpha = 54.7°$, we have pure attractive contact interaction with no DDI, implying zero $\langle L_z \rangle$.

### B. Attractive dipole-dipole interaction

Our main focus in this subsection is to study the formation of vortices in the condensate in the presence of an attractive DDI. For that, we present in Fig. 5 the results for density profiles $|\psi|^2$ of the dipolar $^{164}$Dy BEC. In the upper row of Fig. 5, we first turn off the $s$-wave two-body interaction ($a_s = 0$) to highlight the impact of the DDI when being changed from repulsive to attractive fixing the angular velocity of rotation such that $\Omega = 0.9$. The repulsive DDI is kept maximum in Fig. 5(a) with $\alpha = 0$ such that $a_{dd}\,(0°) = a_{dd} = 131\,a_0$ for the $^{164}$Dy showing a large number of vortices. When we increase the angle $\alpha = 44°$ (reduce the magnitude of repulsive DDI), the number of stable vortices decreases [shown in Fig. 5(b)]. While the DDI is close to zero in Fig. 5(c) with $\alpha = 55°$, the density collapses to such an extent that a single vortex can no longer exist. Next, in the lower row of this figure, we start in Fig. 5(d) by fixing the DDI close to zero as in Fig. 5(c) and adjust the repulsive contact interaction to reproduce the vortex pattern formation previously obtained in Fig. 5(a). This is done primarily to establish a correlation between long-

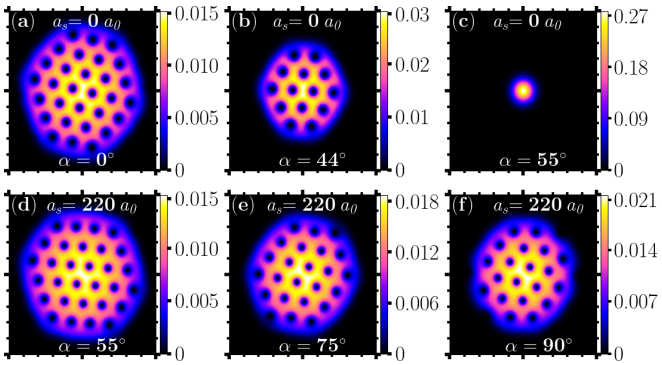


FIG. 5. With the same rotation, panel sizes, and units as in Figs. 2 and 3, here the vortex patterns are shown for dipolar $^{164}$Dy BEC considering (i) $a_s = 0$ (pure dipolar system) in the upper row with a repulsive DDI going from its maximum ($\alpha = 0$) to zero ($\alpha = 55°$) and (ii) $a_s = 220\,a_0$, in the lower row, considering only attractive DDI, from slightly negative (attractive) ($\alpha = 55°$) to maximum attractive ($\alpha = 90°$).

range and short-range interactions in the visual production of vortices in the condensates. Starting with Fig. 5(d), we have Figs. 5(e) and 5(f) to show how far we can reduce the number of vortices by increasing the attractive long-range interaction by changing the angle $\alpha = 90°$ for the $^{164}$Dy condensate. It can be observed from Figs. 5(d)–5(f) that despite introducing maximum attractive DDI, we are able to sustain vortices.

### C. Correlation between long-range DDI and contact interactions on the vortex production

In this section, in Fig. 6, we present a summary of our results highlighting the number of visible vortices ($N_v$) that emerge under a fixed rotation ($\Omega = 0.9$) as we vary the strengths of both DDI and contact interactions from attractive to repulsive domain. This occurs as long as the interactions are suitably balanced ensuring that the net atom-atom

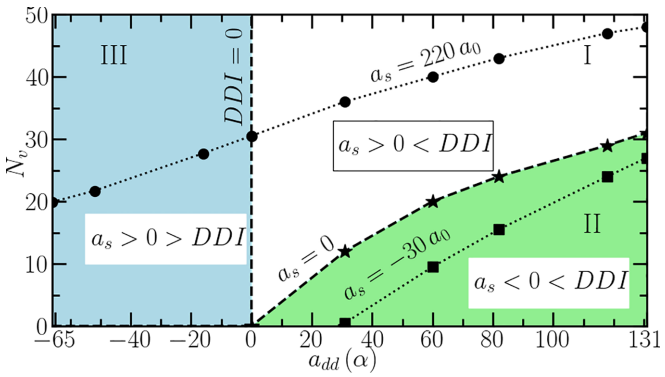


FIG. 6. Number of visible vortices ($N_v$) with rotation being fixed at $\Omega = 0.9$ (units $\omega_\rho$) is plotted against DDI given by (7) (in units of $a_0$). The results are shown for three different values of the contact interaction strengths: $a_s = -30\,a_0$ (squares connected by a dotted line), 0 (starts connected by a dashed line), and 220 $a_0$ (bullets connected by a dotted line). The symbols represent visually identified results (within a possible error of $\pm 1$). Explicitly indicated inside the figure, the colors identify three regions where vortex production can be verified, which are separated by dashed lines.

interaction remains repulsive. In the results shown in Fig. 6, we consider a condensate of $^{164}$Dy as a representative sample as it is the isotope with the largest DDI used in BEC experiments with a maximum DDI given by $a_{dd} = 131\,a_0$. Notably, we observe a correlation between contact and long-range interactions in vortex production when one of them is tuned to zero and the other is sufficiently repulsive. For example, with $a_s = 0$, the number of visible vortices is approximately $N_v \approx 30$ for $a_{dd}\,(0°) = 131\,a_0$ (maximum DDI). Similarly, when $a_{dd} = 0$, $N_v \approx 30$ for $a_s = 220\,a_0$.

The vortex production is directly correlated with the corresponding root-mean-square (rms) radius. Results for the number of vortices ($N_v$) as a function of the DDI are explicitly presented in Fig. 6, considering three fixed strengths of the contact interaction. For attractive contact interactions exemplified by $a_s = -30\,a_0$, the results are represented by box symbols connected with a dotted line. In the case of zero contact interactions ($a_s = 0$), the results are shown as blue star symbols connected by a dashed line. Lastly, for repulsive contact interactions ($a_s = 220\,a_0$), the results are depicted as bullets connected by a solid line. This large repulsive contact interaction was chosen to establish a direct correspondence in the number of visible vortices, $N_v \approx 30$, between the scenario where $a_{dd}(\alpha) = a_{dd}\,(54.7°) = 0$ and the case where the DDI is at its maximum value, $a_{dd}(\alpha) = a_{dd}\,(0°) = 131\,a_0$.

However, this representation can be considered universal as appropriately rescaling the $x$ axis along with the corresponding $N_v$ allows one to describe vortex production for other dipolar species such as $^{168}$Er or $^{52}$Cr. These species have maximum DDIs of $a_{dd}\,(0°) = 66\,a_0$ (with $N_v \approx 20$) and $a_{dd}\,(0°) = 16\,a_0$ (with $N_v \approx 8$), respectively. Therefore, to generalize the results shown in Fig. 6, the diagrams must be rescaled accordingly.

We also find it convenient to identify three distinct regions in the vortex production results, separated by two main dashed lines in the figure (for $a_{dd} = 0$ and $a_s = 0$). Region I (white) corresponds to the case where both interactions are repulsive. Region II (greenish) represents the scenario where the contact interactions are attractive while the DDI remains repulsive. Lastly, region III (bluish) denotes the case where the DDI is attractive, paired with positive (repulsive) contact interactions. To evaluate the relative impact of short-range $s$-wave and long-range DDIs on vortex production, we analyze the variation in the number of vortices, $\Delta N_v$, over a given interval of $a_{dd}(\alpha)$. For example, in Fig. 6, we consider the interval $a_{dd}(\alpha) = 30\,a_0$ to $131\,a_0$, which corresponds to the DDI range in region II where $a_s = -30\,a_0$. In this case, we observe $\Delta N_v = 27$. Using the same interval, $\Delta N_v = 15$ for $a_s = 0$ and $\Delta N_v = 13$ for $a_s = 220\,a_0$. These results clearly demonstrate that repulsive DDIs have a more pronounced effect on vortex production when the contact interactions are attractive. These results indicate that turbulence could be more easily reached by dynamical variations of repulsive DDIs with negative contact interactions.

## IV. CORRELATION BETWEEN DIFFERENT DIPOLAR CONDENSATES

In this section, we attempt to establish a correlation between BECs arising out of the three dipolar atoms that have

TABLE I. Physical quantities and interaction parameters as considered in Figs. 7 (no rotation) and 8 (with rotation given by $\Omega = 0.9$) together with the corresponding numerical results. In the first three rows, as indicated, the results are for $^{164}$Dy, $^{168}$Er, and $^{52}$Cr when maximizing their DDIs ($\alpha = 0$, within their specific independent units). In the fourth and fifth rows, the results are for $^{164}$Dy with $\alpha$ tuned to reproduce approximately the same values of the rms radius previously obtained for $^{168}$Er and $^{52}$Cr respectively (corresponding to the similar vortex patterns presented in Fig. 8).

| BECs | $\alpha$ | $\frac{a_{dd}(\alpha)}{a_0}$ | $\mu(\hbar\omega_\rho)$ | $E(\hbar\omega_\rho)$ | $\sqrt{\langle\rho^2\rangle}(\ell_\rho)$ | $N_v$ |
|---|---|---|---|---|---|---|
| $^{164}$Dy | 0° | 131 | 6.47 | 4.14 | 2.58 | 30 |
| $^{168}$Er | 0° | 66 | 4.62 | 2.98 | 2.16 | 20 |
| $^{52}$Cr | 0° | 16 | 2.35 | 1.60 | 1.53 | 8 |
| $^{164}$Dy | 35° | 66 | 4.63 | 2.98 | 2.16 | 20 |
| $^{164}$Dy | 50° | 16 | 2.33 | 1.58 | 1.52 | 8 |

been considered in cold atom experiments ($^{164}$Dy, $^{168}$Er, and $^{52}$Cr) with reference to the physically observable quantities like energy, chemical potential, vortex number, and rms radius. Using the $^{164}$Dy dipolar BEC as the reference system, we adjust the corresponding orientation of its dipoles relative to the $z$ axis as given by the angle $\alpha$. This adjustment allows the DDI of $^{164}$Dy to be tuned to match with that of the $^{168}$Er and $^{52}$Cr BECs with respect to measurable quantities such as energy, chemical potential, and rms radius. Here, we primarily focus on matching the number of visible vortices to establish a correlation between two different condensates. In this way, by considering $^{164}$Dy as the reference dipolar atomic system and adjusting its DDI through the parameter $\alpha$ appropriately, the same number of vortices of other dipolar atoms like erbium and chromium can be obtained. For example, let us consider $^{52}$Cr being the other atomic species. In this case, we need to tune $\alpha$ such that $a_{dd}(\alpha_{Dy}) = a_{dd}(\alpha) = a_{dd}(\alpha_{Cr} = 0) = 16\,a_0$. In other words, dysprosium at $\alpha = 50°$ is correlated to chromium at $\alpha = 0°$. Using this procedure, the correlation between the observables of the three dipolar atoms in the vortex production is summarized in Table I for pure dipolar condensates (setting $a_s$ to be zero) of $^{164}$Dy, $^{168}$Er, and $^{52}$Cr.

The matching of the number of visible vortices $N_v$ is visually identified by considering the density plots (in which we are ignoring vortices hidden in the low-density regions). This procedure can address any small deviation found in the other observables like energy and chemical potential. As shown, the number of visible vortices is directly proportional to the rms radius. By tuning the dipolar angle of the $^{164}$Dy BEC, such that $\alpha \approx 50°$, its rms radius will be reduced to match with that of a BEC with $^{52}$Cr keeping its DDI to be maximum (i.e., $\alpha = 0°$). Similarly, by adjusting the orientation of the dipoles such that $\alpha = 35°$, the DDI of $^{164}$Dy can be tuned to that of the $^{168}$Er condensate keeping its DDI maximum (i.e., $\alpha = 0°$) so that the number of visible vortices and the rms radius exactly match for both atomic systems.

Related to the results shown in Table I for $a_s = 0$, we also have the density plots shown in Figs. 7 and 8, in which we are comparing the corresponding sizes of the dipolar condensates as well as the vorticity. In Fig. 7, without rotation, the condensate densities obtained for $^{168}$Er [Fig. 7(a)] and $^{52}$Cr [Fig. 7(b)] keeping their DDI maximum are being compared with the densities obtained from $^{164}$Dy in Fig. 7(c) with $\alpha = 35°$ and Fig. 7(d) with $\alpha = 50°$ respectively. In Fig. 8, we present the same four density panels with the rotational frequency given by $\Omega = 0.9$. Therefore, from these results, for pure dipolar systems, it is evident that by appropriately adjusting the orientation of the dipoles relative to the $z$ axis, one observes perfect correlation between the density profiles of the $^{164}$Dy BEC with that of $^{168}$Er and $^{52}$Cr BECs.

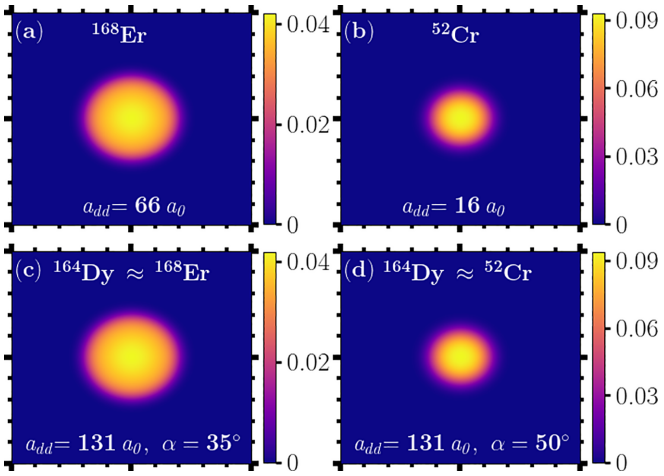


FIG. 7. With no rotation ($\Omega = 0$), zero contact interactions ($a_s = 0$), and maximum DDIs ($\alpha = 0$, in the corresponding independent unit system), in the upper panels, we show the densities of the dipolar BEC systems $^{168}$Er (a) and $^{52}$Cr (b). They are respectively compared with $^{164}$Dy BEC densities, in (d) and (e), by matching their rms radius obtained after tuning the respective dipole orientations. For that, $\alpha = 35°$ in (c) to obtain a correlation with the density of $^{168}$Er (a), whereas $\alpha = 50°$ in (d) to correlate with the density of $^{52}$Cr. The density levels are indicated in bars at the right of the panels with length scales according to the respective atomic condensate that is being considered.

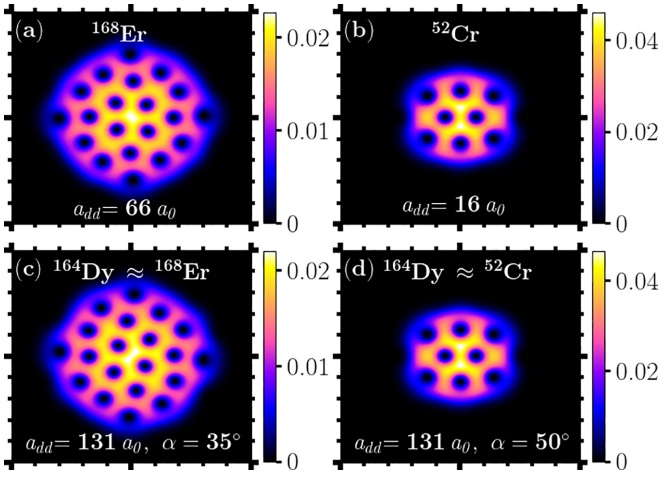


FIG. 8. Following the same as in Fig. 7, but introducing a rotational frequency $\Omega = 0.9$, in units of the transversal trap frequency considered for each specific condensate.

## V. CONCLUSION

In this paper, we explore the generation of energetically stable vortices in a quasi-two-dimensional dipolar BEC endowed with both short- and long-range interactions (contact $s$-wave and DDIs, respectively). We consider a stable configuration with a fixed high rotation close to the transversal trap frequency, $\Omega = 0.9$ (in units of $\omega_\rho$). To achieve this, we first assume an attractive contact $s$-wave interaction ($a_s < 0$) and tune the long-range DDI to be sufficiently repulsive by varying the dipole orientations maximizing the DDI when both dipoles are aligned along the $z$ axis (i.e., $\alpha = 0$). Furthermore, by reversing the roles of the attractive and repulsive interactions, we establish a stable rotating configuration with attractive DDI (for $\alpha > 54.7^\circ$) and repulsive contact interactions ($a_s > 0$). Using the $^{164}$Dy isotope as a reference sample, we investigate the interplay between the long-range DDI and short-range $s$-wave interactions analyzing their relative equivalence in the formation of vortices.

A key result of our paper on the vorticity of a quasi-2D dipolar BEC is the determination of the maximum number of visible vortices achievable for a given contact interaction under high rotation near the transverse rotational frequency of the trap. Our findings show that for a rotation of $\Omega = 0.9$ and zero contact interaction, the maximum number of vortices for $^{164}$Dy (with $a_{dd} = 131\, a_0$) is approximately $N_v \approx 30$. This number can only increase if the DDI exceeds this value, as shown in Fig. 6. Additionally, we observe that vortex production is more pronounced for attractive contact interactions ($a_s < 0$) than for repulsive ones ($a_s > 0$) providing insight into the control and study of quantum turbulence in dipolar BECs.

We have also explored the relationship between dipolar atomic BECs of different species for vortex formation comparing $^{164}$Dy with $^{168}$Er and $^{52}$Cr. By manipulating the orientation of the dipoles, we studied the effects on observable quantities such as the rms radius, energy, and chemical potential (all calculated for zero rotation). Under the same conditions as for $^{164}$Dy, with $a_s = 0$ and $\Omega = 0.9$ (in units of the respective transverse trap frequencies), the maximum number of vortices was found to be $N_v \approx 20$ for $^{168}$Er and $N_v \approx 8$ for $^{52}$Cr.

Our results underscore that vortices can be generated in systems with short-range attractive interactions, provided there is sufficient repulsive long-range DDI. Conversely, vortices can also be produced when the roles of the long- and short-range interactions are reversed with attractive DDIs balanced by sufficiently large repulsive contact interactions. Since the findings of this paper are applicable to other dipolar atomic species, we believe this paper offers a valuable foundation for both theoretical and experimental studies involving rotating dipolar BECs and the exploration of suitable combinations of short- and long-range nonlinear interactions.

## ACKNOWLEDGMENTS

For partial support, S.S. and L.T. thank Fundação de Amparo à Pesquisa do Estado de São Paulo (Grants No. 2020/02185-1, No. 2017/05660-0, No. 2024/04174-8, and No. 2024/01533-7). L.T. also acknowledges partial support from Conselho Nacional de Desenvolvimento Científico e Tecnológico (Grant No. 304469-2019-0). R.R. wishes to acknowledge the financial assistance from DST (Grant No. DST-CURIE-PG/2022/54) and ANRF (formerly DST-SERB) (Grant No. CRG/2023/008153).

[1] P. Kapitza, Viscosity of liquid helium below the λ-point, Nature (London) **141**, 74 (1938).

[2] J. F. Allen and A. D. Misener, Flow of liquid helium II, Nature (London) **141**, 75 (1938).

[3] M. H. Anderson, J. R. Ensher, M. R. Matthews, C. E. Wieman, and E. A. Cornell, Observation of Bose-Einstein condensation in a dilute atomic vapor, Science **269**, 198 (1995).

[4] C. Chin, R. Grimm, P. Julienne, and E. Tiesinga, Feshbach resonances in ultracold gases, Rev. Mod. Phys. **82**, 1225 (2010).

[5] T.-L. Ho, Spinor Bose condensates in optical traps, Phys. Rev. Lett. **81**, 742 (1998).

[6] T. Ohmi and K. Machida, Bose-Einstein condensation with internal degrees of freedom in alkali atom gases, J. Phys. Soc. Jpn. **67**, 1822 (1998).

[7] T. Esslinger, T. W. Hänsch, M. Greiner, O. Mandel, and I. Bloch, Quantum phase transition from a superfluid to a Mott insulator in a gas of ultracold atoms, Nature (London) **415**, 6867 (2002).

[8] A. Griesmaier, J. Werner, S. Hensler, J. Stuhler, and T. Pfau, Bose-Einstein condensation of chromium, Phys. Rev. Lett. **94**, 160401 (2005).

[9] S. H. Youn, M. Lu, U. Ray, and B. L. Lev, Dysprosium magneto-optical traps, Phys. Rev. A **82**, 043425 (2010).

[10] K. Aikawa, A. Frisch, M. Mark, S. Baier, A. Rietzler, R. Grimm, and F. Ferlaino, Bose-Einstein condensation of erbium, Phys. Rev. Lett. **108**, 210401 (2012).

[11] L. Tanzi, E. Lucioni, F. Famà, J. Catani, A. Fioretti, C. Gabbanini, R. N. Bisset, L. Santos, and G. Modugno, Observation of a dipolar quantum gas with metastable supersolid properties, Phys. Rev. Lett. **122**, 130405 (2019).

[12] F. Böttcher, J.-N. Schmidt, M. Wenzel, J. Hertkorn, M. Guo, T. Langen, and T. Pfau, Transient supersolid properties in an array of dipolar quantum droplets, Phys. Rev. X **9**, 011051 (2019).

[13] L. Chomaz, D. Petter, P. Ilzhöfer, G. Natale, A. Trautmann, C. Politi, G. Durastante, R. M. W. van Bijnen, A. Patscheider, M. Sohmen, M. J. Mark, and F. Ferlaino, Long-lived and transient supersolid behaviors in dipolar quantum gases, Phys. Rev. X **9**, 021012 (2019).

[14] T. Koch, T. Lahaye, J. Metz, B. Fröhlich, A. Griesmaier, and T. Pfau, Stabilization of a purely dipolar quantum gas against collapse, Nat. Phys. **4**, 218 (2008).

[15] D. H. J. O'Dell, S. Giovanazzi, and C. Eberlein, Exact hydrodynamics of a trapped dipolar Bose-Einstein condensate, Phys. Rev. Lett. **92**, 250401 (2004).

[16] J. Zhang and H. Zhai, Vortex lattices in planar Bose-Einstein condensates with dipolar interactions, Phys. Rev. Lett. **95**, 200403 (2005).

[17] T. Lahaye, C. Menotti, L. Santos, M. Lewenstein, and T. Pfau, The physics of dipolar bosonic quantum gases, Rep. Prog. Phys. **72**, 126401 (2009).

[18] A. R. P. Lima and A. Pelster, Dipolar Fermi gases in anisotropic traps, Phys. Rev. A **81**, 063629 (2010).

[19] S. Müller, J. Billy, E. A. L. Henn, H. Kadau, A. Griesmaier, M. Jona-Lasinio, L. Santos, and T. Pfau, Stability of a dipolar Bose-Einstein condensate in a one-dimensional lattice, Phys. Rev. A **84**, 053601 (2011).

[20] M. A. Baranov, M. Dalmonte, G. Pupillo, and P. Zoller, Condensed matter theory of dipolar quantum gases, Chem. Rev. **112**, 5012 (2012).

[21] S. Sabari, C. P. Jisha, K. Porsezian, and V. A. Brazhnny, Dynamical stability of dipolar Bose-Einstein condensates with temporal modulation of the s-wave scattering length, Phys. Rev. E **92**, 032905 (2015).

[22] M. O. Borgh, J. Lovegrove, and J. L. Ruostekoski, Internal structure and stability of vortices in a dipolar spinor Bose-Einstein condensate, Phys. Rev. A **95**, 053601 (2017).

[23] S. Sabari and R. K. Kumar, Effect of an oscillating Gaussian obstacle in a dipolar Bose-Einstein condensate, Eur. Phys. J. D **72**, 48 (2018).

[24] S. Sabari and B. Dey, Stabilization of trapless dipolar Bose-Einstein condensates by temporal modulation of the contact interaction, Phys. Rev. E **98**, 042203 (2018).

[25] A. Cidrim, F. E. A. dos Santos, E. A. L. Henn, and T. Macrì, Vortices in self-bound dipolar droplets, Phys. Rev. A **98**, 023618 (2018).

[26] P. C. Diniz, E. A. B. Oliveira, A. R. P. Lima, and E. A. L. Henn, Ground state and collective excitations of a dipolar Bose-Einstein condensate in a bubble trap, Sci. Rep. **10**, 4831 (2020).

[27] L. Chomaz, I. Ferrier-Barbut, F. Ferlaino, B. Laburthe-Tolra, B. L. Lev, and T. Pfau, Dipolar physics: A review of experiments with magnetic quantum gases, Rep. Prog. Phys. **86**, 026401 (2023).

[28] S. Halder, K. Mukherjee, P. K. Panigrahi, S. I. Mistakidis, S. Majumder, S. Das, P. G. Kevrekidis, and H. R. Sadeghpour, Control of $^{164}$Dy Bose-Einstein condensate phases and dynamics with dipolar anisotropy, Phys. Rev. Res. **4**, 043124 (2022).

[29] S. Sabari, Vortex formation and hidden vortices in dipolar Bose-Einstein condensates, Phys. Lett. A **381**, 3062 (2017).

[30] R. Tamil Thiruvalluvar, S. Sabari, K. Porsezian, and P. Muruganandam, Vortex formation and vortex lattices in a Bose-Einstein condensate with Lee-Huang-Yang (LHY) correction, Physica E **107**, 54 (2019).

[31] P. Molignini and B. Chakrabarti, Interaction quench of dipolar bosons in a one-dimensional optical lattice, Phys. Rev. Res. **7**, 013257 (2025).

[32] P. Molignini, Beyond-mean-field phases of rotating dipolar condensates, arXiv:2503.04890.

[33] R. M. Wilson, C. Ticknor, J. L. Bohn, and E. Timmermans, Roton immiscibility in a two-component dipolar Bose gas, Phys. Rev. A **86**, 033606 (2012).

[34] R. K. Kumar, L. Tomio, B. A. Malomed, and A. Gammal, Vortex lattices in binary Bose-Einstein condensates with dipole-dipole interactions, Phys. Rev. A **96**, 063624 (2017).

[35] R. K. Kumar, P. Muruganandam, L. Tomio, and A. Gammal, Miscibility in coupled dipolar and non-dipolar Bose-Einstein condensates, J. Phys. Commun. **1**, 035012 (2017).

[36] A. Trautmann, P. Ilzhöfer, G. Durastante, C. Politi, M. Sohmen, M. J. Mark, and F. Ferlaino, Dipolar quantum mixtures of erbium and dysprosium atoms, Phys. Rev. Lett. **121**, 213601 (2018).

[37] S. Halder, S. Das, and S. Majumder, Two-dimensional miscible-immiscible supersolid and droplet crystal state in a homonuclear dipolar mixture, Phys. Rev. A **107**, 063303 (2023).

[38] N. Bigagli, W. Yuan, S. Zhang, B. Bulatovic, T. Karman, I. Stevenson, and S. Will, Observation of Bose-Einstein condensation of dipolar molecules, Nature (London) **631**, 289 (2024).

[39] M. Lecomte, A. Journeaux, J. Veschambre, J. Dalibard, and R. Lopes, Production and stabilization of a spin mixture of ultracold dipolar Bose gases, Phys. Rev. Lett. **134**, 013402 (2025).

[40] R. K. Kumar, S. Sabari, A. Gammal, and L. Tomio, Rayleigh-Taylor, Kelvin-Helmholtz and immiscible to miscible quenching instabilities in binary Bose-Einstein condensates, arXiv:2503.13767.

[41] A. N. da Silva, R. K. Kumar, A. S. Bradley, and L. Tomio, Vortex generation in stirred binary Bose-Einstein condensates, Phys. Rev. A **107**, 033314 (2023).

[42] L. Klaus, T. Bland, E. Poli, C. Politi, G. Lamporesi, E. Casotti, R. N. Bisset, M. J. Mark, and F. Ferlaino, Observation of vortices and vortex stripes in a dipolar condensate, Nat. Phys. **18**, 1453 (2022).

[43] R. P. Feynman, R. B. Leighton, and M. Sands, *The Feynman Lectures on Physics* (Addison-Wesley, Reading, MA, 1963), Vol. 1, pp. 3–9.

[44] T. Bland, G. Lamporesi, M. J. Mark, and F. Ferlaino, Vortices in dipolar Bose-Einstein condensates, Comptes Rendus Physique **24**, 133 (2023).

[45] L. Khaykovich, F. Schreck, G. Ferrari, T. Bourdel, J. Cubizolles, L. D. Carr, Y. Castin, and C. Salomon, Formation of a matter-wave bright soliton, Science **296**, 1290 (2002).

[46] K. B. Davis, M.-O. Mewes, M. R. Andrews, N. J. van Druten, D. S. Durfee, D. M. Kurn, and W. Ketterle, Bose-Einstein condensation in a gas of sodium atoms, Phys. Rev. Lett. **75**, 3969 (1995).

[47] C. C. Bradley, C. A. Sackett, J. J. Tollett, and R. G. Hulet, Evidence of Bose-Einstein condensation in an atomic gas with attractive interactions, Phys. Rev. Lett. **75**, 1687 (1995); **79**, 1170(E) (1997).

[48] Y. Guo, Y. Luo, and W. Yang, The nonexistence of vortices for rotating Bose-Einstein condensates with attractive interactions, Arch Rational Mech. Anal. **238**, 1231 (2020).

[49] E. Lundh, A. Collin, and K.-A. Suominen, Rotational states of Bose gases with attractive interactions in anharmonic traps, Phys. Rev. Lett. **92**, 070401 (2004).

[50] T. K. Ghosh, Vortex formation in a fast rotating Bose-Einstein condensate, Phys. Rev. A **69**, 043606 (2004).

[51] L. D. Carr and C. W. Clark, Vortices in attractive Bose-Einstein condensates in two dimensions, Phys. Rev. Lett. **97**, 010403 (2006).

[52] S. Sabari, A. Choudhuri, K. Porsezian, and B. Dey, Study of implosion in an attractive Bose-Einstein condensate, Eur. Phys. J. D **70**, 109 (2016).

[53] A. Gammal, T. Frederico, L. Tomio, and Ph. Chomaz, Liquid-gas phase transition in Bose-Einstein condensates with time evolution, Phys. Rev. A **61**, 051602(R) (2000).

[54] A. Gammal, T. Frederico, L. Tomio, and Ph. Chomaz, Atomic Bose-Einstein condensates with three-body interactions and collective excitations, J. Phys. B **33**, 4053 (2000).

[55] S. Sabari, R. K. Kumar, R. Radha, and B. A. Malomed, Interplay between binary and three-Body interactions and enhancement of stability in trapless dipolar Bose-Einstein condensates, Appl. Sci. **12**, 1135 (2022).

[56] S. Giovanazzi, A. Görlitz, and T. Pfau, Tuning the dipolar interaction in quantum gases, Phys. Rev. Lett. **89**, 130401 (2002).

[57] A. Griesmaier, J. Stuhler, T. Koch, M. Fattori, T. Pfau, and S. Giovanazzi, Comparing contact and dipolar interactions in a Bose-Einstein condensate, Phys. Rev. Lett. **97**, 250402 (2006).

[58] S. Sabari, R. K. Kumar, and L. Tomio, Vortex dynamics and turbulence in dipolar Bose-Einstein condensates, Phys. Rev. A **109**, 023313 (2024).

[59] L. Tomio, A. N. da Silva, S. Sabari, and R. K. Kumar, Dynamical vortex production and quantum turbulence in perturbed Bose-Einstein condensates, Few-Body Syst. **65**, 13 (2024).

[60] U. R. Fischer, Stability of quasi-two-dimensional Bose-Einstein condensates with dominant dipole-dipole interactions, Phys. Rev. A **73**, 031602(R) (2006).

[61] D. H. J. O'Dell and C. Eberlein, Vortex in a trapped Bose-Einstein condensate with dipole-dipole interactions, Phys. Rev. A **75**, 013604 (2007).

[62] M. Abad, M. Guilleumas, R. Mayol, M. Pi, and D. M. Jezek, Vortices in Bose-Einstein condensates with dominant dipolar interactions, Phys. Rev. A **79**, 063622 (2009).